Journal of Sound and Vibration 331 (2012) 2856–2873

Contents lists available at SciVerse ScienceDirect

Journal of Sound and Vibration

journal homepage: www.elsevier.com/locate/jsvi

Periodic motions and resonances of impact oscillators

Arcady V. Dyskin [a,*], Elena Pasternak [b], Efim Pelinovsky [c]

[a] School of Civil and Resource Engineering, The University of Western Australia, 35 Stirling Highway, Crawley, WA 6009, Australia
[b] School of Mechanical and Chemical Engineering, The University of Western Australia, 35 Stirling Highway, Crawley, WA 6009, Australia
[c] Institute of Applied Physics, Nizhny Novgorod, Russia

ARTICLE INFO

Article history:
Received 23 April 2011
Received in revised form
19 December 2011
Accepted 25 January 2012
Handling Editor: L.N. Virgin
Available online 24 February 2012

ABSTRACT

Bilinear oscillators – the oscillators whose springs have different stiffnesses in compression and tension – model a wide range of phenomena. A limiting case of bilinear oscillator with infinite stiffness in compression – the impact oscillator – is studied here. We investigate a special set of impact times – the eigenset, which corresponds to the solution of the homogeneous equation, i.e. the oscillator without the driving force. We found that this set and its subsets are stable with respect to variation of initial conditions. Furthermore, amongst all periodic sets of impact times with the period commensurate with the period of driving force, the eigenset is the only one which can support resonances, in particular the multi-'harmonic' resonances. Other resonances should produce non-periodic sets of impact times. This funding indicates that the usual simplifying assumption [e.g., S.W. Shaw, P.J. Holmes, A periodically forced piecewise linear oscillator, Journal of Sound and Vibration 90 (1983) 129–155] that the times between impacts are commensurate with the period of the driving force does not always hold. We showed that for the first sub-'harmonic resonance' – the resonance achieved on a half frequency of the main resonance – the set of impact times is asymptotically close to the eigenset. The envelope of the oscillations in this resonance increases as a square root of time, opposite to the linear increase characteristic of multi-'harmonic' resonances.

1. Introduction

Dynamics of engineering and natural systems often involves return forces which have different magnitudes in tension and compression. One of the main mechanisms of such a difference is the presence of contacts such that the movement in one direction is resisted by the elasticity of the system, while the movement in the other direction involves additional high resistance of the bodies in contact. There are numerous examples of this situation. Firstly, it is characteristic of any cutting process whereby the movement of the cutting tool towards the workpiece creates high contact forces, while the movement away from it meets a lower resistance for the tool holder. This is regarded as the intermittent engagement between the workpiece and the tool and is especially important as it can induce the loss of dynamic stability (chatter) and limit material removal rates especially at high speeds [1]. A particular example is the drill bit–rock interaction whereby the movement of the drill bit away from the rock is resisted by a drill string which is long and hence has low overall stiffness. Also rotations of the cutting tool of the drill bit make the driving force periodic or near periodic. Other examples include mooring lines and towers (e.g., [2–4]), the dynamics of structures with gaps and contacts such as suspension

* Corresponding author.
E-mail address: arcady@civil.uwa.edu.au (A.V. Dyskin).

0022-460X/$ - see front matter © 2012 Elsevier Ltd. All rights reserved.
doi:10.1016/j.jsv.2012.01.031

bridges [5,6], topological interlocking structures [7], where the elements are held together via kinematic constraints rather than a binder, connections of carriages in trains [8], thin cracks in engineering and geo-materials [9–15] as well as biological systems [16]. Another example is the normal oscillations of frictional contacts where the tensile phase of the oscillations reduces normal force and hence friction, such that a sliding increment is possible [17,18]. As a result, the apparent friction controlling the sliding becomes lower than the static one. What is important in these applications is the possibility of resonances in the system which can lead to the loss of stability, for instance via an oscillation-induced reduction in friction.

In this paper, we revisit the theory of bilinear oscillator by considering its simplest form—the impact oscillator. We analyse the periodicity of impact times and the structure of resonances.

A single bilinear oscillator, Fig. 1a and b, is described, after normalisation, by the following equation:

$$x''+2\alpha x'+\tilde{k}(x)x=f(t),\quad \tilde{k}(x)=\begin{cases}\omega_+^2, & x\geq 0\\ \omega_-^2, & x<0\end{cases},\quad \omega_+<\omega_- \tag{1}$$

where $x(t)$ is the trajectory of the oscillator, α is the damping coefficient. We note that given the driving force $f(t)$ is continuously differentiable, solution of (1) is twice continuously differentiable while its third derivative is discontinuous at $x=0$. Often $f(t)$ is considered to be periodic. In some cases the driving force also has an additional constant component (pre-loading, e.g., [5,18]).

The main feature of the bilinear oscillator is that the phase space is split into two regions (states) within which the oscillator behaves linearly, while the nonlinearity is associated with crossing the boundary between the linear states. The resonant frequency can be obtained by summing up the times oscillator spent in each of the linear state; the result is (e.g., [19])

$$\Omega_r=\frac{2\Omega_+\Omega_-}{\Omega_++\Omega_-},\quad \Omega_\pm^2=\omega_\pm^2-\alpha^2 \tag{2}$$

System (1) and its stability were investigated in detail for the case of harmonic excitation when $f(t)=A\cos(\omega t+\varphi)$ (e.g., [2,7,16,19–21]). The main results are obtained by the semi-analytical method using the analytical solutions for the linear states with transition points determined as the closest (in time) solution of a certain nonlinear algebraic equation (see the general theory in Wiercigroch [22]). An alternative is to employ direct numerical methods of solving the corresponding differential equations (e.g., [5]).

It was shown that system (1) exhibits multi-harmonic ($\omega=n\Omega_r$) and sub-harmonic resonances ($\omega=(1/m)\Omega_r$), where n, m are integers. These frequencies are also seen in the corresponding spectra (e.g., [14,7]). Subharmonic (multi-harmonic) resonances were experimentally detected in materials with cracks and defects by Solodov and Korshak [23] and Solodov et al. [24,25]. Based on this, an apparatus was proposed by Ohara et al. [26] to use subharmonic ultrasound for the accurate imaging of closed cracks. Phase portraits resembling the ones associated with bilinear oscillators were observed in the milling experiment [1]. Multiple peak spectra were observed in a cracked beam [11] and in stacked (unglued) concrete and mortar blocks under impact load [27].

The abrupt transition from one value of the stiffness to another reduces the smoothness of the solution, especially if the transition point $x\neq 0$. Subsequently, some authors modelled the bilinear oscillator by smoothing the force–displacement (stress–strain) curves. Lyakhovsky et al. [12] model the dynamics of rocks with bilinear behaviour (different moduli in tension and compression) by using a constitutive law which essentially rounds the kink shown in Fig. 1b. This of course makes the solution smooth, but then the solution becomes dependent upon the radius of rounding, which in its own turn depends upon the parameters of the model. Given the presence of regions of instability in bilinear oscillators, it is yet unclear whether the smoothened model will converge to the original bilinear one as the radius tends to zero. Peng et al. [15,28] approximated the bilinear oscillator by a nonlinear one with a polynomial dependence of the stiffness upon the displacement. The polynomial is chosen in such a way that the natural frequencies of the bilinear oscillator (1) and its approximation are closely matched. This method is however only applicable to low frequency ratios, i.e. when the

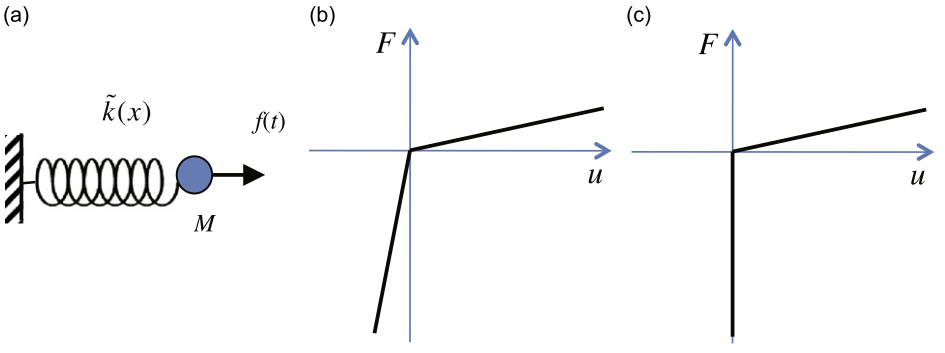

Fig. 1. Bilinear oscillator: (a) oscillator with nonlinear spring; (b) the return force law for bilinear oscillator; and (c) the return force law for impact oscillator.

stiffnesses differ slightly and the oscillator is close to the linear one (the smallest frequency ratio modelled in [15,28] was 0.8). This approach could be viewed as an extension of the modelling of a bilinear oscillator with small difference in stiffnesses with a linear one mentioned by Miles [29]. In the cases when the difference in stiffnesses is high, this approach is clearly not applicable.

Another feature of the bilinear oscillator is the existence of regions of instability and chaotic behaviour (e.g., [2,3,5,6,19,20,30,31]). In particular, this manifests itself in instabilities in the numerical solution [18]. Shaw and Holmes [19] performed stability analysis of both bilinear and impact ($\omega_- \to \infty$, Fig. 1c) oscillators. Whiston [20] extended this analysis to the case of bilinear oscillator with preload. Their analysis is based on the assumption that the flight time

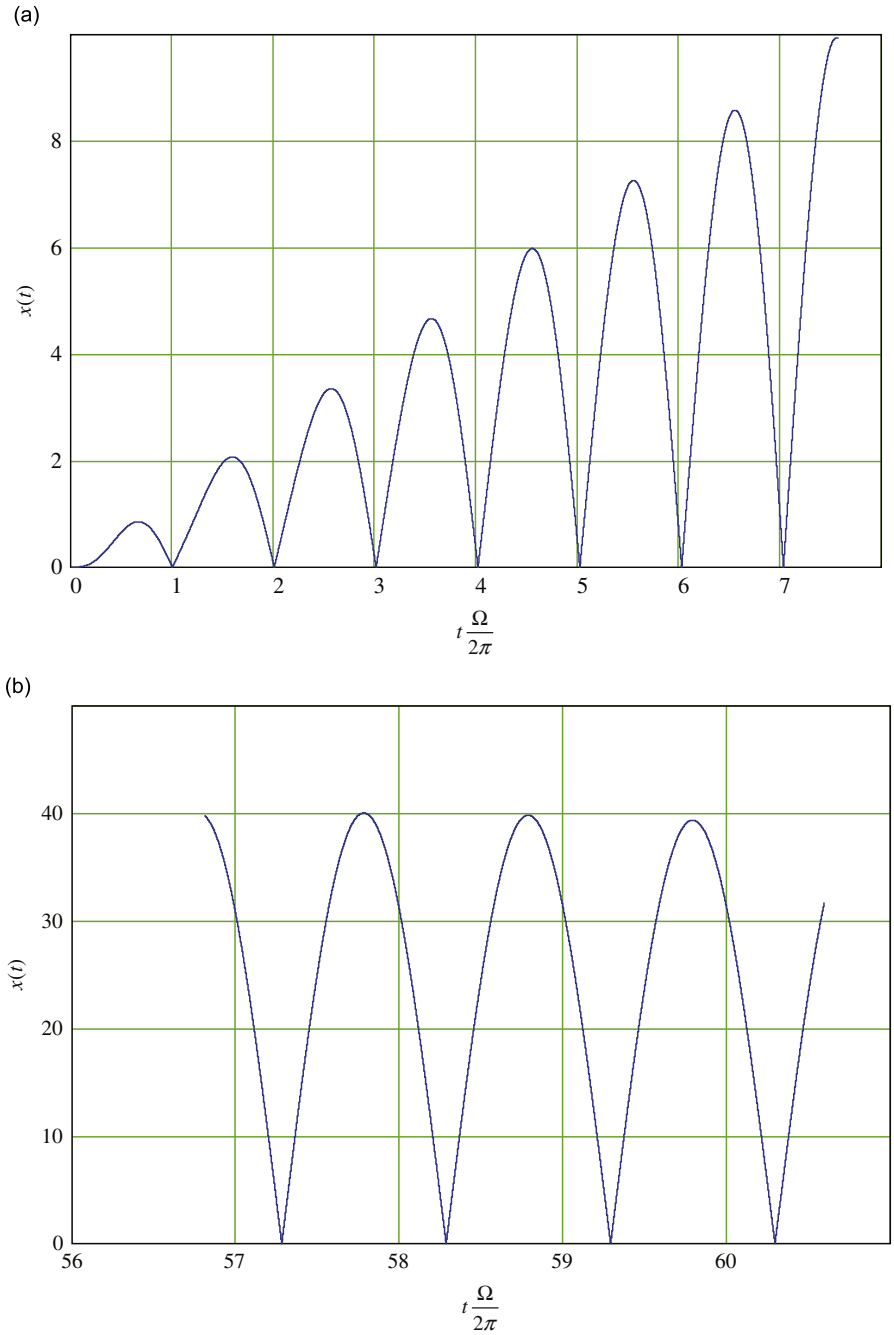

Fig. 2. The numerical solution of (1) with $\omega_-^2/\omega_+^2 = 20$ showing the displacement of the impact oscillator without damping ($\alpha = 0$) with the driving force having frequency 1 percent higher than the resonance one ($\omega = 1.01\Omega_r$). Plots show only the beginning (a) and the end (b) of the time interval $[0,\ 60\Omega_r/2\pi]$.

(the time between the successive transitions from $x>0$ to <0) is commensurate to the period of driving force. For the case of impact oscillator this assumption would mean that the set of impact times has a period equal or multiple to the period of the driving force. While for harmonic driving forces with the frequency ω multiple of the eigenfrequency of the oscillator ($\omega=K\Omega_r$) it is valid, any minor deviation from such a frequency will produce non-periodic impact times, as illustrated by Fig. 2. It is seen that while in the beginning (Fig. 2a) the intervals between the successive impacts seem to be equal to the period of the driving force, eventually at the end of the time interval (Fig. 2b) the non-periodicity becomes apparent.

The above overview shows that it is necessary to conduct further analysis in an attempt to determine the possibility of closed form solutions. The only known analytical solutions are those which correspond to the limiting case of $\omega_-\to\infty$, Fig. 1c. This is so-called impact oscillator[1] (e.g., [19]) whose multi-harmonic resonances ($\omega=n\Omega_r$) were found in closed form [2,16,19].

Here we concentrate on the impact oscillator without damping and with the coefficient of restitution equal to 1. We approach the problem by analysing the sets of impact times. We start with formulating general properties of impact oscillators (Section 2) and specific properties related to the respective sets of impact times (Section 3). In Section 4 we consider the periodic impact times commensurate with the excitation period, derive the multi-harmonic resonances and determine the conditions for periodic motion. In Section 5 we consider the first subharmonic resonance and analyse its asymptotical behaviour.

2. Impact oscillator and its properties

The limiting transition $\omega_-\to\infty$ transfers (1) to

$$x''+2\alpha x'+\omega_+^2 x=f(t),\quad x>0 \tag{3}$$

Points $x(t)=0$ are the transition (impact) points happening at times t_k, $k=0, 1,\ldots$, where

$$x(t_k)=0,\quad x'(t_k+0)=-x'(t_k-0)=V_k \tag{4}$$

and V_k are impact velocities. Formally, (3), and (4) can be solved stepwise starting with initial conditions at t_0 and using the conventional solution of linear equation to which (3) turns in the interval (t_0, t_1). Point t_1 is determined from equation $x(t_1)=0$. Then for the interval (t_1, t_2) the velocity at point t_1+0 is determined from (4) and again the conventional solution is used, and so on. Thus for given initial conditions the solution of (3) and (4) exists and unique.

In order to further simplify the analysis we assume the absence of damping, $\alpha=0$. By setting $\alpha=0$, rewriting (3) and (4) in terms of the dimensionless time variable $t\to t\omega_+$ and denoting f/ω_+^2 as just f, one obtains the following differential equation:

$$x''+x=f(t),\quad x>0, \tag{5}$$

which is to be solved together with impact conditions (4).

The resonance frequency of (5) is $\Omega_r=2$ in the dimensionless time variable; correspondingly the multi-harmonics are even numbers, $2n$. It is also easy to see that if $f(t)$ is infinitely differentiable, the solution $x(t)$ is infinitely differentiable in the intervals (t_k, t_{k+1}), where $\{t_k\}$ is the set of impact times. At the impact times the first derivative $x'(t)$ and all odd derivatives $x^{(2m+1)}(t)$, $m=1, 2, \ldots$ are discontinuous, while the solution itself, $x(t)$ and all even derivatives $x^{(2m)}(t)$, $m=1, 2, \ldots$ are continuous.

We also note that while the differential operator in the left hand side of (5) is nonlinear, it allows a limited form of convex combination, namely if $x(t)$ and $y(t)$ satisfy $x''+x=f(t)$, $x>0$ and $y''+y=g(t)$, $y>0$ with *the same impact times* $\{t_k\}$, then for any $\alpha, \beta>0$ $z=\alpha x+\beta y$ satisfies equation

$$z''+z=\alpha f(t)+\beta g(t),\quad z>0 \tag{6}$$

together with conditions (4) at the impact points. This property trivially follows from the fact that both $x(t)$ and $y(t)$ are not negative and have the same zeros, $\{t_k\}$, so their convex combination is positive, has the same zeros and satisfies (6) in between them.

It is seen from this property that the sets of impact times play a pivotal role in the structure of solutions of system (5) with conditions (4). This suggests that the impact oscillator can be analysed by considering sets of impact times and corresponding impact velocities, which are of course the points of the Poincaré map for $x=0$ (e.g., [19]). In what follows we pursue this approach.

3. Impact times

We introduce the following notations. Let $\Theta=\{t_k\}$ be a set of impact times. We shift the origin to the first impact time such that $t_0=0$. We single out a special set $\Theta_0=\{\pi k\}$, $k=0, 1,\ldots$ which is the set of impact times for solutions of

[1] It should be noted that the term 'impact oscillator' is also used to indicate rigid body impacting systems (see e.g. [32,33] and literature reviews [34,35]). We use the term here as a synonym of asymptotics of large ratios of stiffnesses on compression and tension in a bilinear oscillator, as introduced by Shaw and Holmes [19].

homogeneous equation

$$x''+x=0, \quad x>0, \tag{7}$$

with impact conditions (4) and initial conditions

$$x(0)=0, \quad \dot{x}(0)=V_0 \tag{8}$$

where V_0 is the initial velocity. We will call set $\Theta_0=\{\pi k\}$ the *eigenset* of Eq. (7). The solution of Eq. (7) with impact conditions (4) and initial conditions (8) can be expressed as

$$x_0(t)=V_0\sin(t-\pi k) \text{ for } \pi k\le t\le \pi(k+1) \tag{9}$$

Obviously, if x is a solution of (5) with the set of impact times $\Theta_0=\{\pi k\}$, then $x+x_0$ is another solution (but with a different initial velocity). Thus x_0 plays a role of a neutral element in a semigroup of solutions of non-homogeneous equation (5) with the set of impact times $\Theta_0=\{\pi k\}$. This is an analogue of the corresponding relation between homogeneous and non-homogeneous linear differential equations.

We now list some properties of (5) and (4) related to the sets of impact times.

Property 1. *If x and $y\neq x$ satisfy $x''+x=f(t), \quad x>0$ and $y''+y=g(t), \quad y>0$ with the same impact times $\Theta\subset\Theta_0$, then $f\neq g$. (We assume that neither $f\equiv 0$ nor $g\equiv 0$.) In other words the decomposition of the solution into the sum of a general solution of homogeneous equation and a particular solution of the heterogeneous one is only possible for solutions with impact times belonging to the eigenset $\Theta_0=\{\pi k\}$. Thus, if $\Theta\subset\Theta_0$, then the solution of the homogeneous equation cannot be added to the solution of the corresponding non-homogeneous equation without changing the driving force, contrary to the case of linear differential equations.*

Proof. Suppose the opposite is valid, $f=g$. Then, due to uniqueness of the solution of (5) and (4) for any k, $x'(t_k)\neq y'(t_k)$, otherwise x and y would coincide. Suppose $x'(t_k)=V_k$, $y'(t_k)=W_k$ and let $V_k<W_k$. Consider interval (t_k, t_{k+1}). Since, in this interval, both x and y satisfy the same linear differential equation (7) with the same right hand side, $z(t)=y(t)-x(t)$ is a solution of the corresponding homogeneous equation on (t_k, t_{k+1}) with initial conditions $z(t_k)=0$, $z'(t_k)=W_k-V_k$. The form of this solution is known, it is $z(t)=(W_k-V_k)\sin t$. Since both x and y have the next zero at t_{k+1}, this point must be a zero of z. Therefore, $t_{k+1}=t_k+\pi s_k$, where s_k is integer, which implies that $\Theta\subseteq\Theta_0$. This concludes the proof.

This property has another interpretation: for an equation with the given right hand side changing the initial velocity leads to change in the set of impact times Θ as long as $\Theta\subset\Theta_0$.

Given that Θ_0 is the set of impact times for the general solution of homogeneous equation that satisfies (4), one could think that Property 1 applies to any set $\Theta\neq\Theta_0$. This is however not so, since there exist sets Θ such that changing initial velocity, at least in a certain interval does not affect Θ. This is demonstrated by the following example.

Example: Consider the following set of impact times:

$$\Theta_m=\{\pi s_k\}\subset\Theta_0: s_0=0, \quad s_{k+1}=\begin{cases} s_k+m & \text{if } k \text{ is even} \\ s_k+1 & \text{if } k \text{ is odd} \end{cases} \tag{10}$$

and a family of functions

$$x_*(t)=A\sin t-\cos\frac{2t+\pi}{m+1}+\cos\frac{\pi}{m+1} \tag{11}$$

All these functions have Θ_m as a set of their roots. At all other points they satisfy (5) with

$$f(t)=\frac{(3-m)(m+5)}{(m+1)^2}\cos\frac{2t+\pi}{m+1}+\cos\frac{\pi}{m+1} \tag{12}$$

The factor A is to be chosen in each interval between the impact times to ensure that the obtained solution of (5) and (12) is not negative. In order to accomplish this we note that set Θ_m has period $T=(m+1)\pi$. The first part of (11) (the solution of homogeneous equation in the linear case) has period either T or $2T$ for m odd or even, respectively. Let V_0 be the initial velocity (at $t=0$). Then

$$A=\begin{cases} V_0+\frac{2}{m+1}\sin\frac{\pi}{m+1} & \text{if } 0\le t\le m\pi \\ -V_0+\frac{2}{m+1}\left[1+2(-1)^m\right]\sin\frac{\pi}{m+1}, & \text{if } m\pi\le t\le(m+1)\pi \end{cases} \tag{13}$$

For the next interval $(m+1)\pi\le t\le 2(m+1)\pi$ the initial velocity is

$$V_1=\begin{cases} -V_0+\frac{4}{m+1}\sin\frac{\pi}{m+1}, & \text{if } m \text{ is even} \\ V_0, & \text{if } m \text{ is odd} \end{cases} \tag{14}$$

When m is even, the initial velocity becomes equal to V_0 only for the next interval $2(m+1)\pi\le t\le 3(m+1)\pi$, which reflects the fact that in this case the period is $2(m+1)\pi$.

Figs. 3 and 4 show functions (11) and (13) for $m=2$ and 3. These functions deliver the solutions of (5) and (12) with impact times Θ_m for some values of initial velocity V_0. However, not all values V_0 produce solutions of (5) and (12) with the

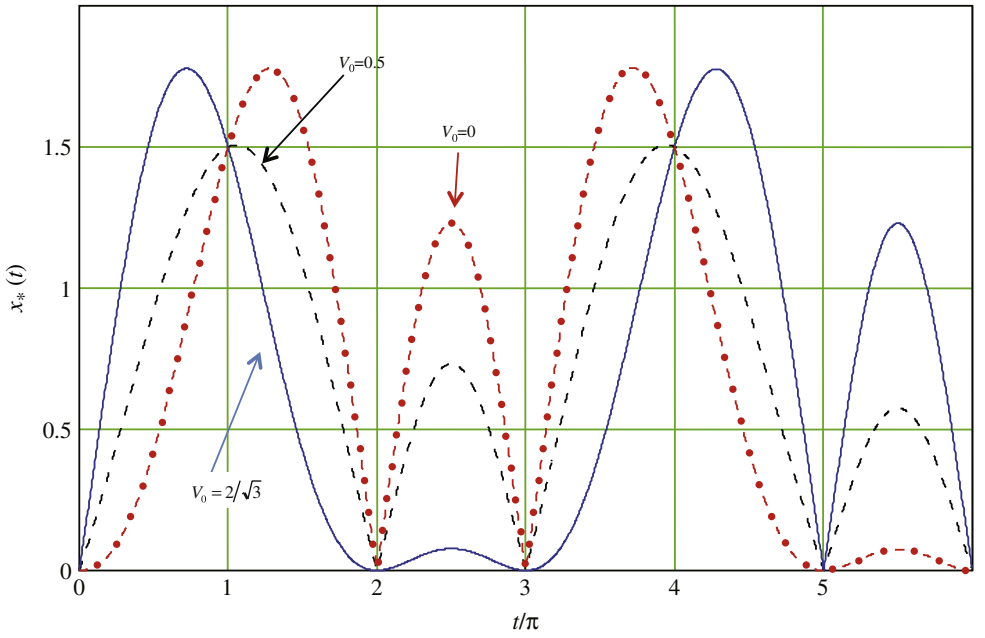

Fig. 3. Trajectory (11) and (13) of impact oscillator for impact times Θ_m (the example) for $m=2$ and different values of V_0. The initial velocity $V_0 = 2/\sqrt{3}$ is the maximal velocity at which the impact times remain Θ_m.

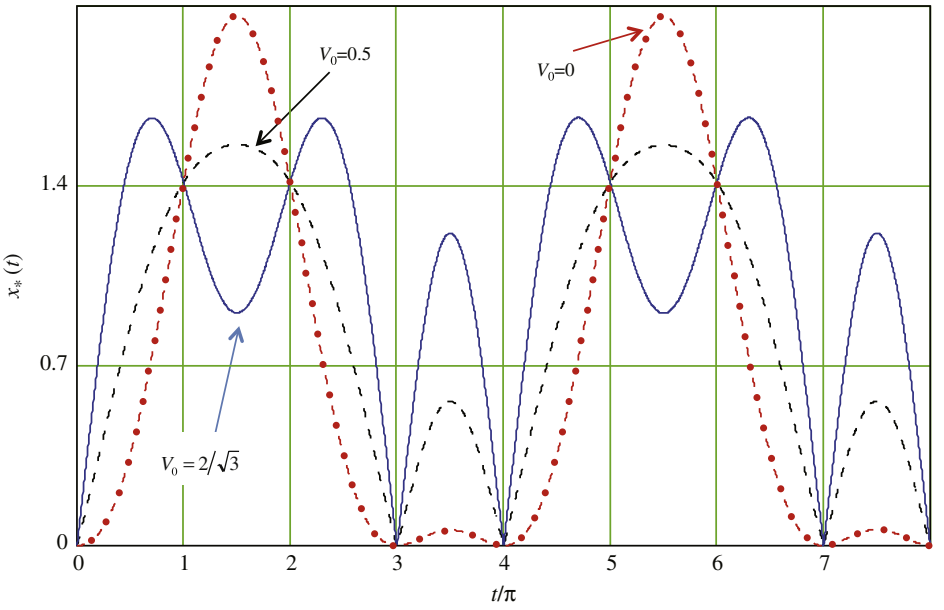

Fig. 4. Trajectory (11) and (13) of impact oscillator for impact times Θ_m (the example) for $m=3$ and the same values of V_0 as in Fig. 3.

set of impact times Θ_m. The condition is $V_0 < V_*(m)$, where for even m, $V_*(m) = (4/(m+1))\sin(\pi/(m+1))$. For $m=3$, $V_*(3) = 1+3/4\sqrt{2}$. For other odd values of m, $V_*(m)$ are given in Table 1 (see Appendix A for details). For values of V_0 higher than $V_*(m)$ the solutions of (5) and (12) still exist, but involve different (irregular) sets of impact times.

It is noteworthy that while for $m=3$ the period is $(m+1)\pi$, which coincides with the period of the driving force, for $m=2$ the period is as twice as much, $2(m+1)\pi$.

The example considered demonstrates that the periods of impact times and the driving force do not have to coincide (the impact times may even be aperiodic) contrary to the assumption made in [19,20]. It also highlights the importance of

Table 1
Limiting values of initial velocity below which there exist solutions of (5) and (12) with impact times Θ_m.

m	5	7	9	11	13	15
$V_*(m)$	1.5	0.984	0.675	0.486	0.365	0.283

a case when both the set of impact times and the driving force are periodic and share a common period. This case is analysed in the following section.

4. Periodic impact times commensurate with the excitation period: Resonances

Assume now that the set Θ of impact times is periodic with a period T and that the driving force has the same period, $f(t+T)=f(t)$. Then for a resonance to happen the set of impact times must coincide with the eigenset Θ_0 as assured by the following property:

Property 2. *If a solution x of (5) with impact times Θ is a resonance, then $\Theta=\Theta_0$.*

Proof. Suppose the opposite holds and $\Theta\neq\Theta_0$. Let $x(t)$ be a solution of (5) with initial condition $x'(0)=V_0$ and suppose that it is a resonance, i.e. $x'(t_k+T)>x'(t_k)$ and for any V there exists impact time $t_V\in\Theta:\ x'(t_V)>V$. As usual, we assume that $t_0=0$.

We conduct the proof in the following steps.

1. We show that for any k and the impact velocities, $V_n=x'(t_k+nT)$ and for any m there exist $n>m$ such that $V_n>V_m$. Indeed, suppose $V_n=V_m$ and let $V=\max\limits_{[mT,(m+1)T]}x'(t_k+t)$ then choose n such that $t_{2V}\in[t_k+nT,\ t_k+(n+1)T]$. Introduce $x_m(t)=x(t+t_k+mT)$ and $x_n(t)=x(t+t_k+nT)$. They are both solutions of (5) with the T-periodic driving force and have the same initial conditions by the assumption, so they must coincide. However, this contradicts the way they were constructed in which $x_n'(t)>2x_m'(t)$. Thus $V_n>V_m$.
2. We now have two solutions of the same equation with different initial velocities. According to Property 1, $\Theta\subset\Theta_0$, at least when the origin is moved to t_k.
3. We show that $V_n\to\infty$ as $n\to\infty$. Again, assume the opposite that the set of impact velocities $\{V_n\}$ is bounded, i.e. there exists W such that $0\le V_n\le W$. Then there exists a subsequence $\{V_{n_i}\}\subset\{V_n\}$ which converges to a limit. That means that for any $\varepsilon>0$ there exists N such that for any $i,\ j>N:\ |V_{n_i}-V_{n_j}|<\varepsilon$. We now introduce two solutions, $y(t)=x(t+n_iT)$ and $z(t)=x(t+n_jT)$. In the interval $(t_k,\ t_{k+1})$ we represent these two solutions as
$$y(t)=A_y\sin t-x_{\mathrm{part}}(0)+x_{\mathrm{part}}(t)$$
$$z(t)=A_z\sin t-x_{\mathrm{part}}(0)+x_{\mathrm{part}}(t) \tag{15}$$
where $x_{\mathrm{part}}(t)$ is a partial solution of non-homogeneous equation (5) in its linear state, $A_y=V_{n_i},\ A_z=V_{n_j}$. Obviously, $|A_y-A_z|<\varepsilon$ and subsequently, for $t\in[t_k,\ t_{k+1}]$
$$|y(t)-z(t)|<\varepsilon \text{ and } |y'(t)-z'(t)|<\varepsilon \tag{16}$$
It follows from here that $|y'(t_{k+1})-z'(t_{k+1})|<\varepsilon$ and then inequalities (16) can be continued by induction into the full period T. On the other hand, n_j can be chosen large enough to contain point t_{2V}, where $V=\max_{[t_k,t_k+T]}y'(t)$, which contradicts (16).
4. We can now prove Property 2. Indeed, due to the supposition $\Theta\neq\Theta_0$, there exists an interval $(t_k,\ t_{k+1})$ such that $t_{k+1}-t_k=s_k\pi,\ s_k>1$. We use representation of the type of (15) in this interval and since the interval is longer than π, there are points t, where $A\sin t<0$. On the other hand, by shifting t_k by the large enough number of periods we can ensure that $|A\sin t|>2\max|x_{\mathrm{part}}(t)|$, which violates the condition $x(t)\ge0$. Thus assumption $\Theta\neq\Theta_0$ leads to a contradiction, and hence $\Theta=\Theta_0$. This concludes the proof.

Property 2 is a necessary condition of resonance on a periodic set of impact times. This is however not a sufficient condition as demonstrated below by the analysis of the equation
$$x''+x=\sin nt,\quad x>0 \tag{17}$$
Period of the driving force here is $2\pi/n$. When n is even, the period of eigenset Θ_0 (recall, it is π) is equal to or a multiple of $2\pi/n$. Then the resonance is possible and its form is well known (e.g., [2,19]):
$$x_k(t)=A_k\sin t-\frac{1}{n^2-1}\sin nt,\quad x_k'(t)=A_k\cos t-\frac{n}{n^2-1}\cos nt \tag{18}$$

$$A_k=(-1)^k\left[V_k+\frac{n}{n^2-1}\right],\quad V_k=V_{k-1}+\frac{2n}{n^2-1}, \tag{19}$$

where $V_k>0$ is the impact velocity at the beginning of a cycle.

This is a multi-harmonic resonance (since the main angular frequency of oscillator (17) is 2) with linearly increasing amplitude and impact velocity. The higher the harmonics, the smaller velocity increment V_k-V_{k-1}; it decreases as $2/n$. Fig. 5 shows solutions (18) and (19) for $n=2$, 4, 6.

When however n is odd, only the double period of eigenset Θ_0 (which is 2π) is equal to or a multiple of $2\pi/n$. Formally, the necessary condition of resonance is satisfied, but direct calculations show that the solution with impact times Θ_0 is

$$x_k(t)=A_k\sin t-\frac{1}{n^2-1}\sin nt,\quad x_k'(t)=A_k\cos t-\frac{n}{n^2-1}\cos nt,\quad A_k=(-1)^kV_k+\frac{n}{n^2-1} \tag{20}$$

It follows from here that

$$V_k=V_{k-1} \tag{21}$$

Thus we have steady-state oscillations (Fig. 6a). This solution is however only valid as long as $x_k(t)$ does not have roots (impact times) in addition to the elements of eigenset Θ_0. From (20) we obtain the following equations for the extra roots:

$$\text{For } k=2p\quad \left[V_{2p}+\frac{n}{n^2-1}\right]\sin t-\frac{1}{n^2-1}\sin nt=0,\quad 2p\pi<t<(2p+1)\pi \tag{22}$$

$$\text{For } k=2p+1\quad \left[-V_{2p}+\frac{n}{n^2-1}\right]\sin t-\frac{1}{n^2-1}\sin nt=0,\quad (2p+1)\pi<t<2(p+1)\pi \tag{23}$$

Since $V_k>0$, Eq. (22) does not have roots in the interval $(2p\pi, 2p\pi+\pi)$. Consider interval $(2p\pi+\pi, 2p\pi+2\pi)$. In order to find the values of V_k, which allow the extra roots, we use the same technique as in Appendix A. We consider V_k as a parameter and starting with a large value of V_k, keep reducing it until an extra root appears. Let t_* be the extra root. This obviously happens at the point when $x_k(t_*)=x_k'(t_*)=0$. This leads to a system of equations which, after substitution $t_*=\xi+2p\pi+3\pi/2$, $-\pi/2\le\xi\le\pi/2$, assumes the form

$$\begin{cases} x(\xi)=\left[V_{2p}-\frac{n}{n^2-1}\right]\cos\xi+\frac{(-1)^m}{n^2-1}\cos n\xi=0,\quad n=2m+1\\ x'(\xi)=\left[V_{2p}-\frac{n}{n^2-1}\right]\sin\xi+\frac{(-1)^m n}{n^2-1}\sin n\xi=0 \end{cases} \tag{24}$$

Due to the symmetry, it is sufficient to consider $0\le\xi\le\pi/2$. The analysis, similar to the one conducted in Appendix A, shows that for $n=3$ the suitable root of (24) is $\xi=0$. (The other root, $\xi=\pi/2$, gives a trivial condition $V_k\ge 0$.) From here the condition of the existence of extra roots is $V_k=V_{2p}\le V_{\max}=1/2$. For $n=5, 7,\ldots$ system (24) reduces to equation

$$\tan\xi=n\tan n\xi \tag{25}$$

Then the condition of the existence of extra roots is

$$V_k=V_{2p}\le V_{\max}\frac{1}{n^2-1}\left[n-(-1)^m\frac{\cos n\xi}{\cos\xi}\right],\quad n=2m+1 \tag{26}$$

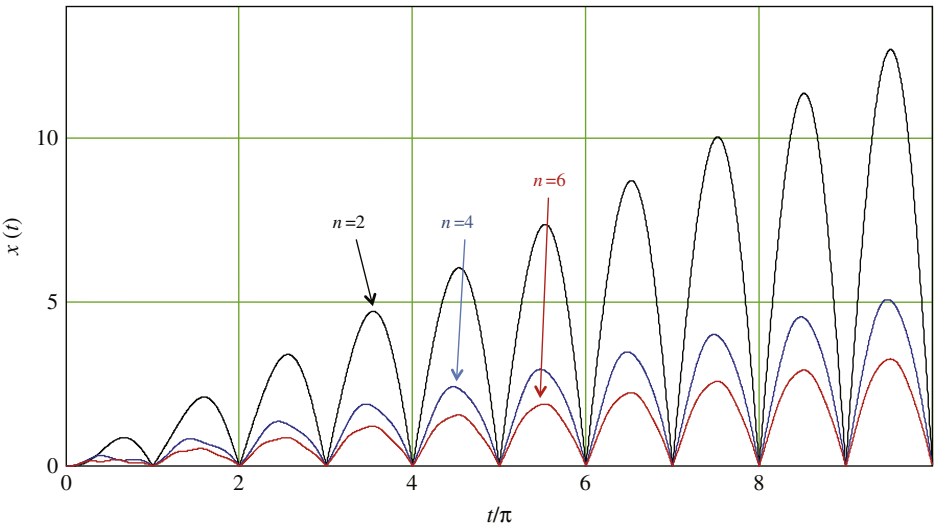

Fig. 5. Trajectories (18) and (19) of impact oscillator with multi-harmonic driving force showing the main resonance ($n=2$), double ($n=4$) and triple ($n=6$) resonances.

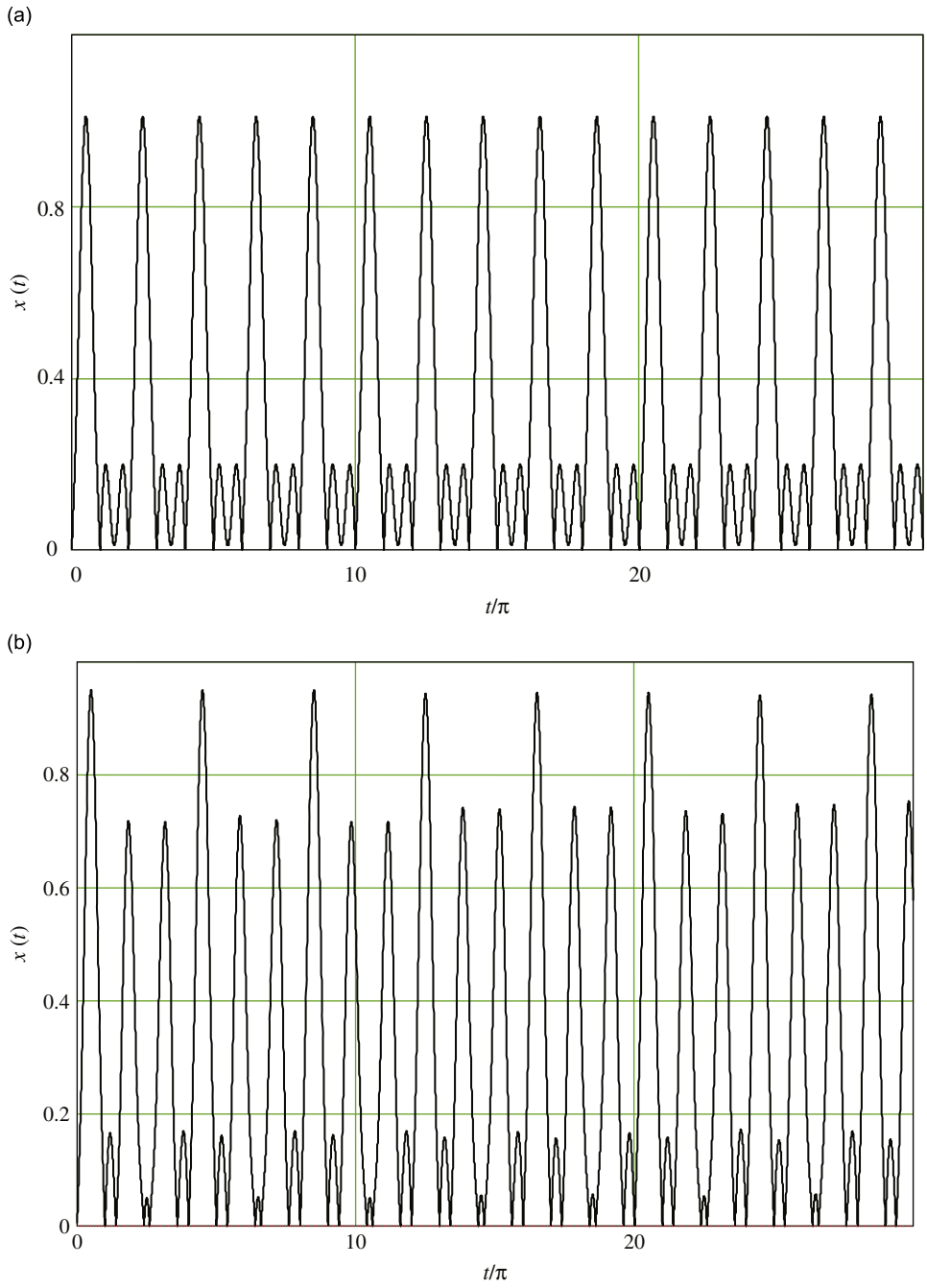

Fig. 6. Numerically calculated trajectories of impact oscillator (17) with a periodic driving force for $n=3$ (3/2 harmonic) with different initial velocities: (a) $V_0=0.51$ (impact times Θ_0, Eq. (20)) and (b) $V_0=0.45$ (impact times $\Theta\neq\Theta_0$).

Eq. (25) was solved numerically and the upper bounds were produced for impact velocities shown in Table 2.

As an example, Fig. 6b shows solutions of (17) for $n=3$ and $V_0=0.51$ (which corresponds to impact times Θ_0, Fig. 6a) and $V_0=0.45$ (impact times different from Θ_0, Fig. 6b). These values of V_0 are chosen because the first one is greater than $V_{\max}=\frac{1}{2}$ and the second one is smaller than that. The first plot is the trajectory according to (20). The second plot was obtained numerically using the fourth-order Runge–Kutta method adaptive step to solve the corresponding bilinear oscillator equation (1) with $\alpha=0$, $\omega_-/\omega_+=2\times10^4$ and 2^{20} points in the interval $(0, 30\pi)$. The difference in behaviour for different initial velocities is also seen in the phase portraits (Fig. 7), and power spectra $|S(\omega)|^2$ (Fig. 8), where $S(\omega)$ is Fourier transform of $x(t)$. In particular, the solution with periodic impact times shows regular spectral peaks of rapidly reducing

Table 2
Critical values of initial velocity. Velocities below the critical one produce solutions of (17) with impact times different from the eigenset Θ_0.

n	5	7	9	11	13	15
$V_{max}(n)$	0.26	0.18	0.138	0.112	0.095	0.082

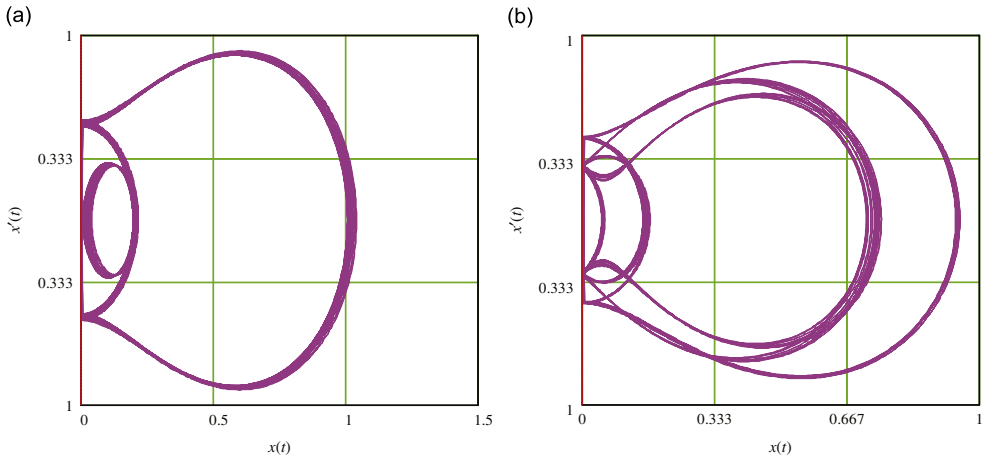

Fig. 7. Phase portraits of impact oscillator (17) with a periodic driving force for $n=3$ (3/2 harmonic) with different initial velocities: (a) $V_0=0.51$ (impact times Θ_0, Eq. (20)) and (b) $V_0=0.45$ (impact times $\Theta \neq \Theta_0$).

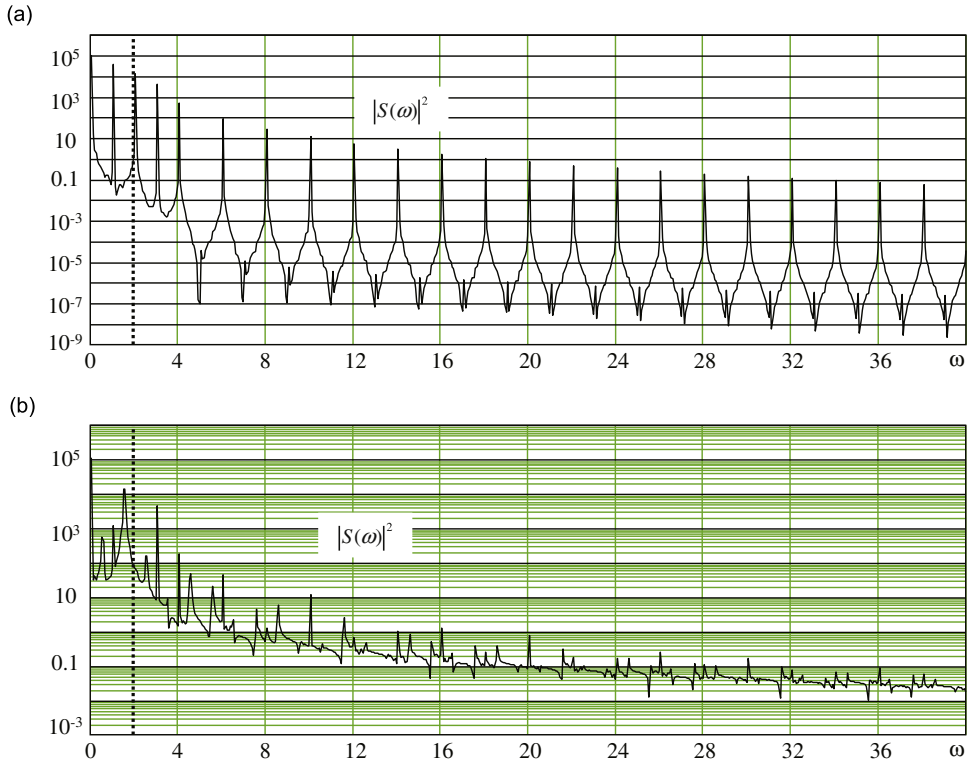

Fig. 8. Power spectra of impact oscillator (17) with a periodic driving force for $n=3$ (3/2 harmonic) with different initial velocities: (a) $V_0=0.51$ (impact times Θ_0, Eq. (20)) and (b) $V_0=0.45$ (impact times $\Theta \neq \Theta_0$). The vertical line $\omega=2$ indicates the resonant frequency of the oscillator.

amplitude as frequency increases, while the other solution is characterised by a wider spectrum with irregular but much slower reduced spectral peaks.

For comparison, Fig. 9 shows another case when impact times are Θ_0—periodic motion for $n=9$ and $V_0=0.139$.

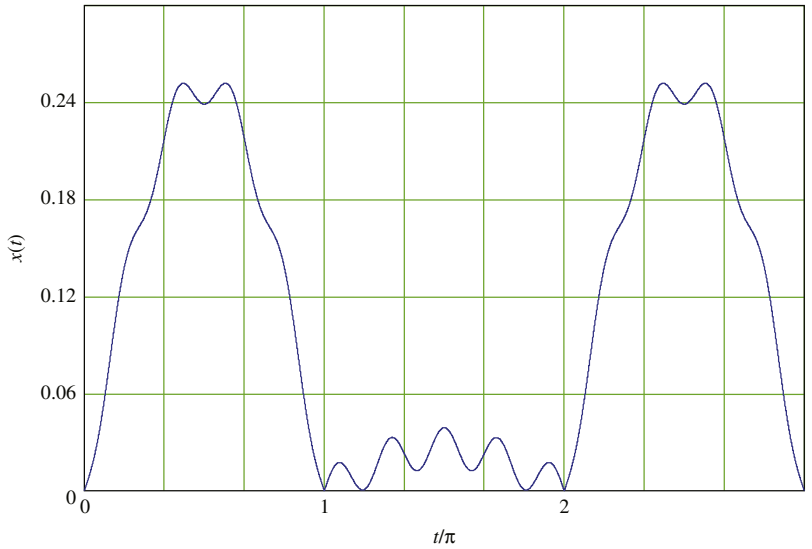

Fig. 9. Numerically calculated trajectories of impact oscillator (17) with a periodic driving force for $n=9$ (9/2 harmonic) with initial velocity $V_0=0.139$ (impact times Θ_0).

Thus, the only resonances with periodic impact times commensurate with the period of driving force are the ones given by (18) and (19). We will now turn our attention to resonances not associated with the eigenset of impact times Θ_0. These are subharmonic resonances.

5. Asymptotically periodic impact times: Subharmonic resonance

Consider excitation on the half harmonic frequency (the main resonant frequency is equal to 2):

$$x''+x=\sin t, \quad x>0 \tag{27}$$

Numerical simulations show [2,3,19] that this equation exhibits resonance, which we will now analyse.
Let $\Theta=\{t_k\}$ be a set of impact times. For each interval (t_k, t_{k+1}) we can express the solution of (27) as

$$x_k(t)=A_k\sin t+B_k\cos t-\frac{t}{2}\cos t$$
$$x_k'(t)=\left(A_k-\frac{1}{2}\right)\cos t-B_k\sin t+\frac{t}{2}\sin t \tag{28}$$

Suppose both the impact time t_k and the impact velocity V_k are known. Then Eq. (28) give the motion for $t>t_k$ and the next impact time, t_{k+1}, is to be found from equation $x_k(t_{k+1})=0$. This equation, by introducing $\xi_k=t_{k+1}-t_k$ (which is the period at cycle k) can be written in the form

$$\tan\xi_k=\frac{\cos t_k}{\cos t_k+2V_k}\xi_k \tag{29}$$

This equation cannot be solved analytically, however asymptotics of large V_k which corresponds to the half harmonic resonance can be found as follows. We denote

$$\frac{\cos t_k}{\cos t_k+2V_k}=\alpha_k \tag{30}$$

and note that for $V_k\gg 1\,|\alpha_k|\ll 1$. Then the asymptotic solution of (29) can be expressed as

$$\xi_k=\pi(1+\alpha_k)+O(\alpha_k^2), \quad \alpha_k=\frac{\cos t_k}{2V_k}+O(V_k^{-2}), \tag{31}$$

Therefore, at large V_k the impact time period is close to π and the set of impact times $\Theta=\{t_k\}$ is asymptotically close to the eigenset Θ_0.

We can now express the impact velocity for the next cycle as $V_{k+1}=-x_k'(t_{k+1})$. After some algebra we have

$$V_{k+1}=V_k+\frac{\pi}{2}[\sin t_k+(\pi+2\sin t_k)\alpha_k]+O(\alpha_k^2) \tag{32}$$

Now, t_k is close to $k\pi$ but in order to express the difference one needs the velocity from the previous cycle, V_{k-1}. Instead, we just proceed to the next cycle and find that

$$V_{k+2} = V_k + \frac{\pi}{2}\frac{[(\pi/2)\cos^2 t_k + \sin 2t_k]}{V_k} + O(V_k^{-2}) \tag{33}$$

Now, using the approximation $V_{k+2} - V_k = (t_{k+2} - t_k)V'(t_k) = 2\pi(1+\alpha_k)V'(t_k) + O\left(V_k^{-2}\right)$, considering times much larger than $t_{k+2} - t_k$, and replacing the numerator in (33) with its average value which we denote a ($a > 0$ as we assume resonance), one obtains the following differential equation for asymptotics $V(t)$:

$$\frac{dV}{dt} = \frac{a}{\pi V} + O(V^{-2}) \tag{34}$$

Solution of (34), together with the assumption that $V(0)=0$ is

$$V(t) = b\sqrt{t} \tag{35}$$

where b is a constant. Fig. 10 shows $x'(t)$ obtained through the numerical solution of (27) with the initial condition $V_0=0$. We used the fourth-order Runge–Kutta method adaptive step for the corresponding bilinear oscillator equation (1) with $\alpha=0$, $\omega_-/\omega_+ = 2\times 10^4$and 2^{20} points in the interval (0, 400). The plot also shows asymptotics (35), where constant b is determined by making (35) the envelope of the velocity plot. Fig. 11 shows that the same power law provides the envelope for $x(t)$ as well. In both cases the fact that the numerical solution allows asymptotics (35) indicates that for these values of parameters the numerical solution is accurate.

Figs. 12 and 13 show the phase portrait and power spectrum. Both the phase portrait and power spectrum have a regular character with the power spectrum showing strong regular peaks. This is attributed to the fact that the set of impact times is asymptotically regular approaching Θ_0 as the impact velocities increase.

The existence of the half harmonic resonance depends upon the phase of the driving force. As an example consider the equation

$$x'' + x = \cos t, \quad x > 0 \tag{36}$$

The general solution for each interval (t_k, t_{k+1}) has the form

$$\begin{aligned} x_k(t) &= \left(A_k - \frac{t}{2}\right)\sin t \\ x_k'(t) &= \left(A_k - \frac{t}{2}\right)\cos t - \frac{1}{2}\sin t \end{aligned} \tag{37}$$

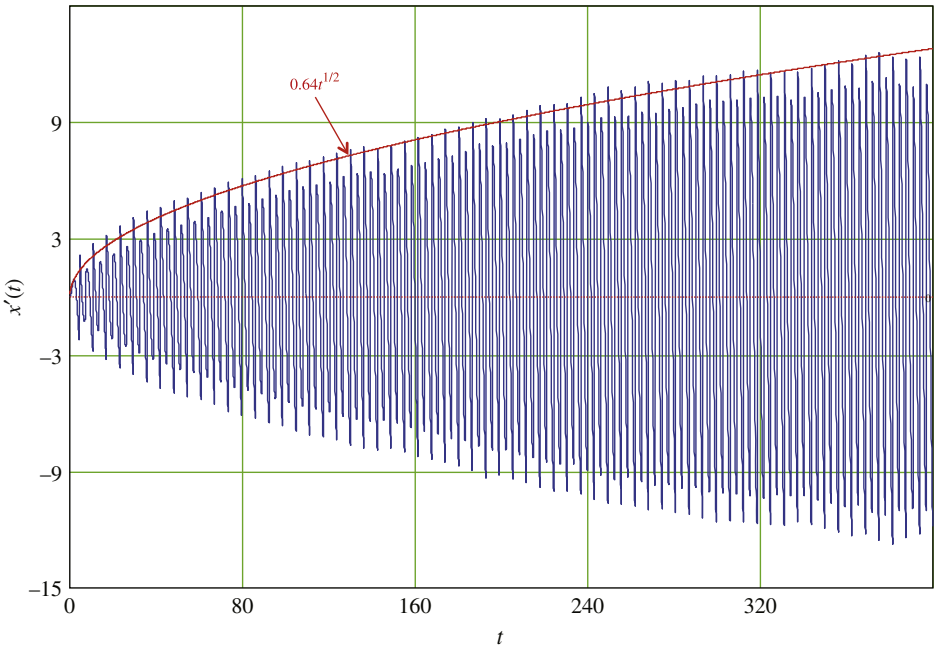

Fig. 10. Velocity obtained through numerical modelling of impact oscillator (27) with driving force at half harmonic frequency. The envelope represents asymptotics (35).

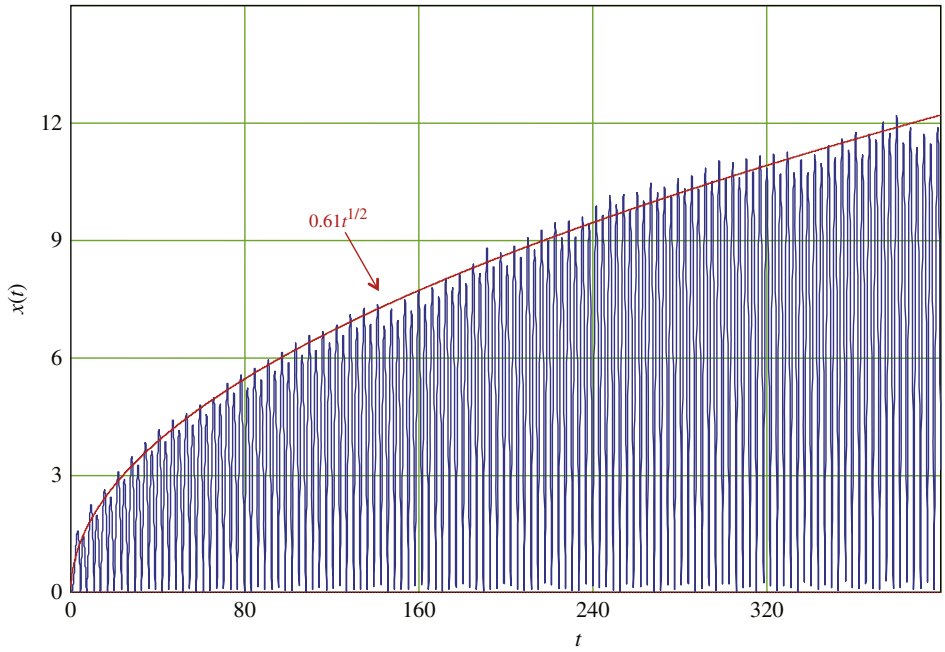

Fig. 11. Displacement obtained through numerical modelling of impact oscillator (27) with driving force at half harmonic frequency. The envelope represents asymptotics (35).

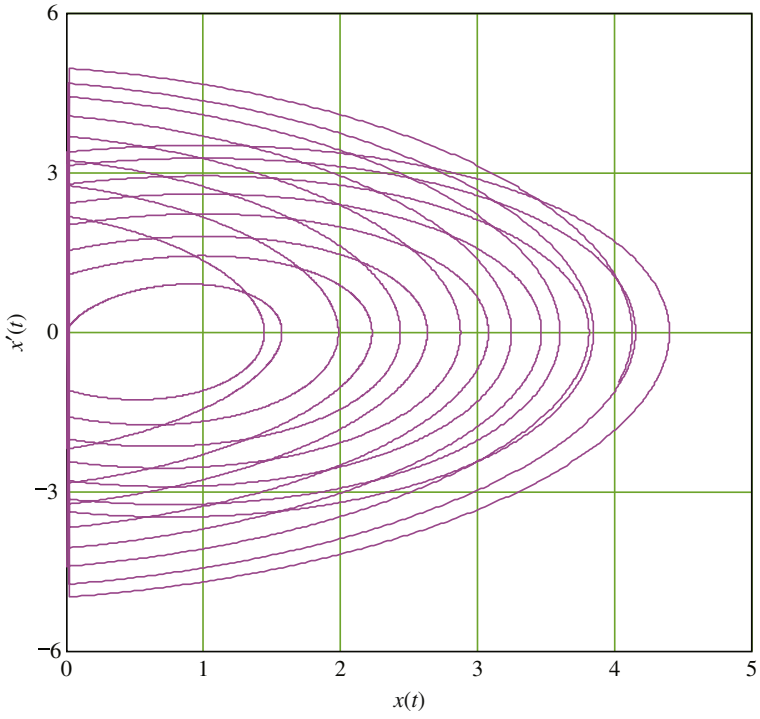

Fig. 12. Phase portrait of impact oscillator (27) with driving force at half harmonic frequency.

The obvious set of impact times to test is Θ_0, since $x_k(k\pi)=0$. If V_k is the impact velocity at $k\pi$, then (37) produce the following set of solutions:

$$x_k(t)=\left(V_k+(-1)^k\frac{\tau}{2}\right)\sin\tau,\quad \tau=t-k\pi,\quad 0\le\tau\le\pi$$
$$x_k'(t)=\left(V_k+(-1)^k\frac{\tau}{2}\right)\cos t-\frac{(-1)^k}{2}\sin t \tag{38}$$

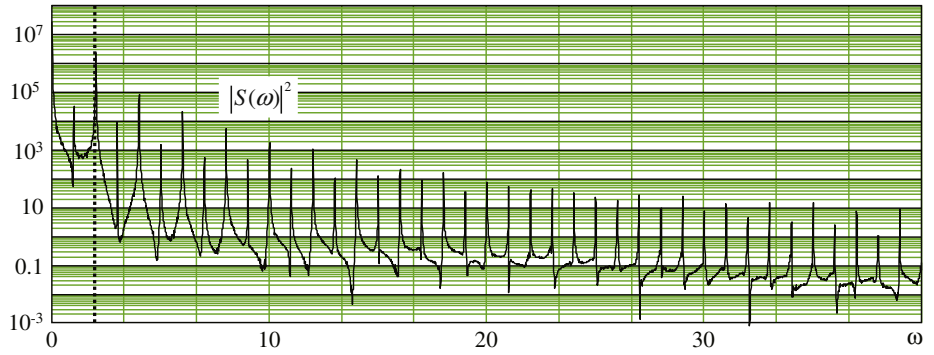

Fig. 13. Power spectrum of impact oscillator (27) with driving force at half harmonic frequency. The vertical line $\omega=2$ indicates the resonant frequency of the oscillator.

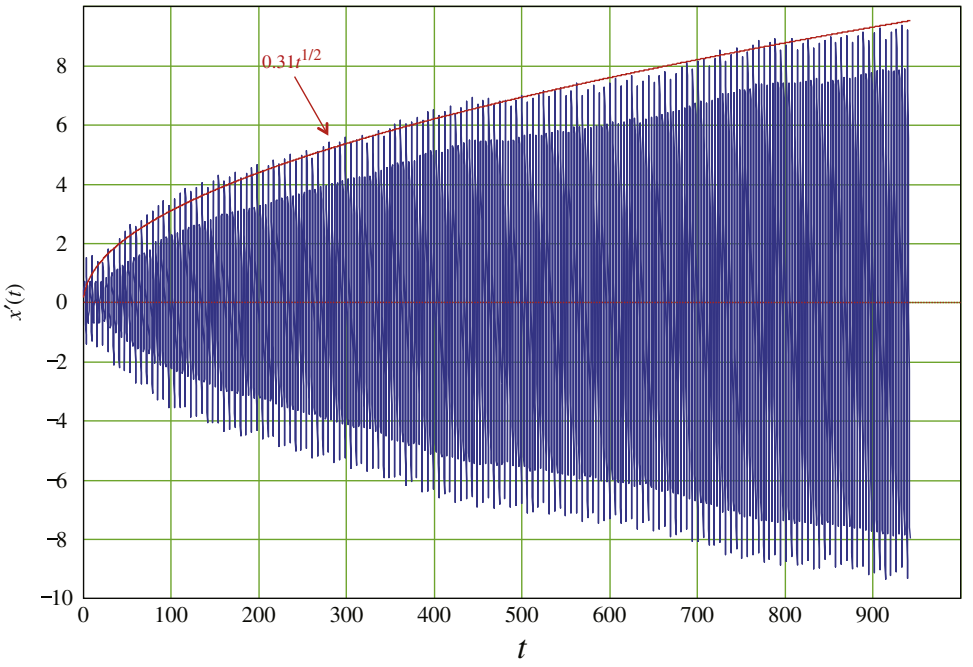

Fig. 14. Velocity obtained through numerical modelling of impact oscillator (36) with zero initial velocity. The envelope represents asymptotics (35).

From here

$$V_{k+1}=V_k+(-1)^k\frac{\pi}{2},\quad V_{k+2}=V_k \tag{39}$$

It is now necessary to check if there are any additional solutions of $x_k(t)=0$. To this end we rewrite the first equation of (38) as

$$x_k(t)=\left(V_k+\frac{\tau}{2}\right)\sin\tau,\quad \text{if } k \text{ is even},$$

$$x_k(t)=\left(V_k-\frac{\tau}{2}\right)\sin\tau,\quad \text{if } k \text{ is odd},$$

$$\tau=t-k\pi,\quad 0\le\tau\le\pi \tag{40}$$

It is seen, that for even k the only solutions are $k\pi$. For odd k the additional solutions are only possible if $V_k\le\pi/2$. On the other hand, the first equation of (39) states that for odd k, $V_k\ge V_{k-1}+\pi/2\ge\pi/2$, since all $V_k\ge 0$. Therefore, the only situation when other solutions are possible is $V_0=0$. Then, there is an impact time at $t=\pi/2$.

Thus for any initial velocity $V_0>0$, Eq. (36) has only steady-state periodic solutions with periodic impact times Θ_0. If however $V_0=0$, one can shift time by $\pi/2$ to place the origin in this additional impact time. This will turn Eq. (36) into (27)

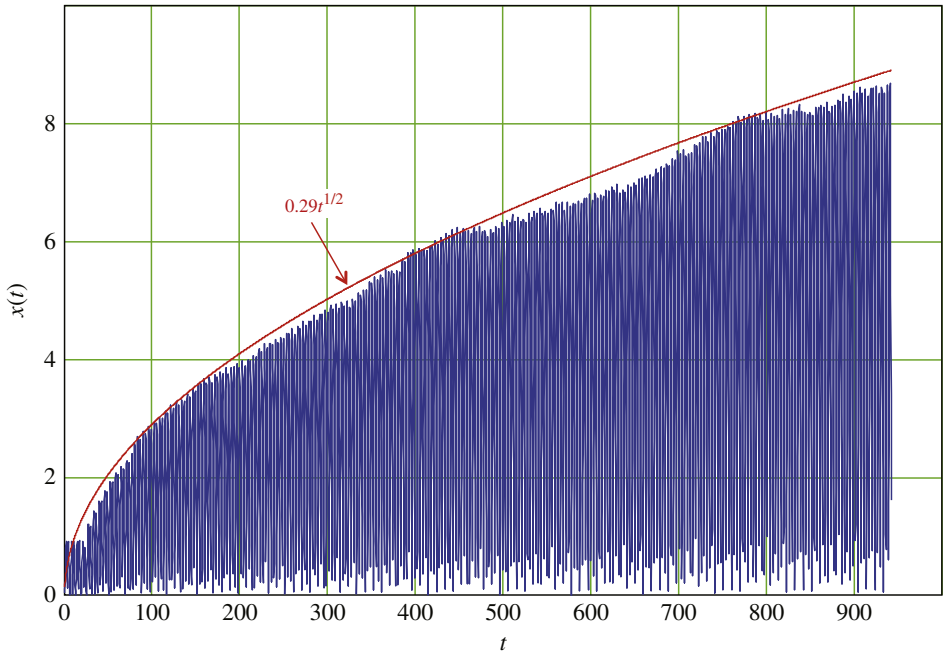

Fig. 15. Displacement obtained through numerical modelling of impact oscillator (36) with zero initial velocity. The envelope represents asymptotics (35).

and the corresponding analysis applies. Figs. 14 and 15 show the corresponding velocity and displacement vs. time. The envelopes show the same asymptotics (35), but the factors are now much lower owing to the time shift.

6. Discussion

We have considered the bilinear oscillator with stiffness transition at zero displacement in its simplest form—impact oscillator which corresponds to the case when stiffness in compression is taken as infinity. The trajectory of the impact oscillator is non-negative and assumes zero only at certain time points called impact times. The velocities change sign at the impact times, while the absolute values remain the same. (The coefficient of restitution is assumed to be equal to unity.) Closed form solutions are known for only few cases, so numerical modelling has been the only tool in analysing the impact oscillators. However, when the combinations of parameters are such that the oscillator exhibits chaotic behaviour, the numerical simulation is not stable. Developing a general theory of impact oscillators is hampered by the fact that the solutions of the equations modelling impact oscillators are not additive, unless they share the same sets of impact times. Thus the sets of impact times play pivotal role in the impact oscillator motions and should be used as a basis of the analysis of impact oscillators.

Amongst all sets of impact times, there is a special one which can be regarded as the eigenset, that is the set of impact times corresponding to the solution of the homogeneous equation, i.e. the oscillator without the driving force. The importance of it is in the fact that this set and its subsets are the only ones that can support different motions of impact oscillator for different initial conditions. With all other sets of impact times, any change in the initial velocity will change the impact times.

An important feature of impact oscillator is the presence of multiple resonances, both sub- and multi-'harmonic'. The eigenset of impact times plays a special role here as well: amongst all periodic sets of impact times with the period commensurate with the period of driving force, the eigenset is the only one which can support resonance. Subsequently, the multi-'harmonic' resonances are the ones supported by the eigenset. Other resonances produce non-periodic sets of impact times. It is interesting that for the first sub-'harmonic resonance' – a resonance achieved on a half frequency of the homogeneous equation – the set of impact times is not periodic; it is however asymptotically close to the eigenset. The envelope of the oscillations in this resonance increases as a square root of time, opposite to the linear increase characteristic of multi-'harmonic' resonances.

The eigenset of impact times and its periodic subsets also support steady-state periodic oscillations. Their existence however strongly depends upon the initial conditions (magnitude of impact velocity)—there exist ranges of initial velocities which produce oscillations with the eigenset of impact times (or its periodic subsets), while outside these ranges the impact times lose periodicity.

7. Conclusion

We analysed the motions of impact oscillators with impacts at zero displacement, the full restitution and periodic driving force. Such oscillators model a wide range of phenomena, from oscillations of fragmented structures and mooring lines, to chatter in cutting tools, to deformation of geological media. We performed the analysis by considering the associated sets of impact times – the times of change of the velocity sign. We singled out the eigenset – the impact times of a free oscillator (the oscillator without the driving force). This is a periodic set and this is the only set which supports multi-harmonic resonances independent of the initial velocities. In all other cases, the periodic impact times commensurate with the period of the driving force, if exist depend upon the initial velocity. This means that the traditional approach to analysing the stability of bilinear oscillators based on Poincare maps related to times which are multiple of the driving force period is insufficient, as some important cases (e.g., subharmonic resonances) are missed.

We also analysed the first subharmonic resonance (half of the resonance frequency) and found that the set of impact times, while not periodic, is asymptotically close to the eigenset. The envelope of the oscillations in this resonance increases as a square root of time, opposite to the linear increase characteristic of multi-'harmonic' resonances.

Acknowledgements

The authors acknowledge the financial support from the Australian Research Council through the Discovery Grant DP0988449.

Appendix A. Upper bounds for initial velocities which deliver solutions of (5) and (12) with impact times Θ_m

Here we derive bounds on V_0 which ensure that solution (11), (13) and (14) is non-negative. To this end we rewrite the solution taking into account the periodicity:

$$x_*(t)=u(t)-w(t),$$

$$u(t)=\begin{cases}\left(V_0-\frac{2}{m+1}\sin\frac{\pi}{m+1}\right)\sin t, & 0\le t\le m\pi\\ \left(-V_0+\frac{2}{m+1}\left(1+2(-1)^m\right)\sin\frac{\pi}{m+1}\right)\sin t, & m\pi\le t\le (m+1)\pi\end{cases}$$

$$w(t)=\cos\frac{2t+\pi}{m+1}-\cos\frac{\pi}{m+1} \tag{A1}$$

The condition $x_*(t)\ge 0$ is satisfied when

$$u(t)\ge w(t) \tag{A2}$$

Fig. A1 shows the plots for both $u(t)$ and $w(t)$ for even m (Fig. A1a) and odd m (Fig. A1b). For $m\pi<t<(m+1)\pi$ and for all values of t when m is even, condition (A2) can be reduced to

$$|u'(t)|\ge|w'(t)|, \tag{A3}$$

which produces the condition on V_0

$$V_0<V_*(m)=\frac{4}{m+1}\sin\left(\frac{\pi}{m+1}\right) \tag{A4}$$

For $0<t<m\pi$ and odd values of m the upper bound $V(m)$ can be determined from the condition that plots $u(t)$ and $w(t)$ touch each other at a certain point t_*. For $m=3$ this point is obviously in the middle of interval $(0, m\pi)$ (Fig. A1b), that is $t_*=3\pi/2$. Then the condition $x_*(t_*)=0$ leads to

$$V_*(3)=1+3\sqrt{2}/4 \tag{A5}$$

For other odd values of m, t_* is determined from the solution of the system for D and t_*

$$\begin{cases}D\sin t_*-\cos\frac{2t_*+\pi}{m+1}+\cos\frac{\pi}{m+1}=0\\ D\cos t_*+\frac{2}{m+1}\sin\frac{2t_*+\pi}{m+1}=0\end{cases} \tag{A6}$$

where D is an (unknown) amplitude of $u(t)$ at which plots $u(t)$ and $w(t)$ touch each other, $(m-2)\pi\le t_*\le(m-1)\pi$. Then the upper bound for V_0 can be found from the condition that the amplitude of $u(t)$ does not exceed D:

$$V_0-\frac{2}{m+1}\sin\frac{\pi}{m+1}\le D, \tag{A7}$$

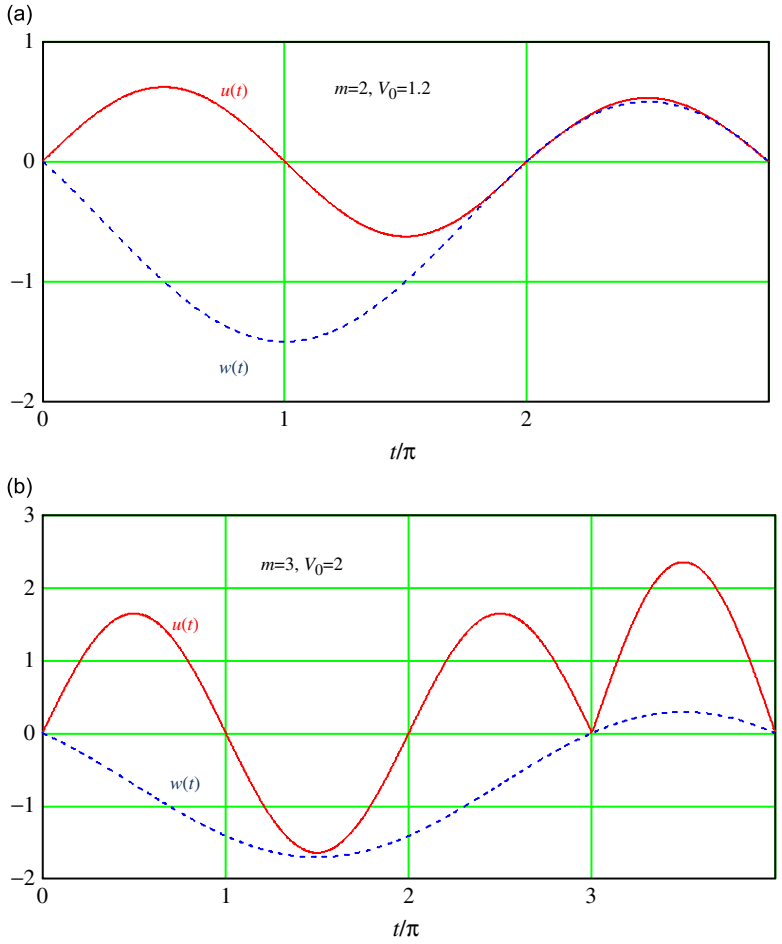

Fig. A1. Illustration to solving inequality (A2): (a) even m and (b) odd m.

from where the upper bound can be expressed through t_*

$$V_*(m)=\frac{2}{m+1}\left[\sin\frac{\pi}{m+1}-\frac{\sin\left((2t_*+\pi)/(m+1)\right)}{\cos t_*}\right] \tag{A8}$$

The tangent point t_* was found by solving system (A6) numerically; the results are shown in Table 1.

References

[1] M.A. Davies, B. Balachandran, Impact dynamics in milling of thin-walled structures, *Nonlinear Dynamics* 22 (2000) 375–392.
[2] J.M.T. Thomson, Complex dynamics of compliant off-shore structures, *Proceedings of the Royal Society of London A* 387 (1983) 407–427.
[3] J.M.T. Thompson, A.R. Bokaian, R. Ghaffari, Subharmonic resonances and chaotic motions of a bilinear oscillator, *IMA Journal of Applied Mathematics* 31 (1983) 207–234.
[4] M. Gerber, L. Engelbrecht, The bilinear oscillator: the response of an articulated mooring tower driven by irregular seas, *Ocean Engineering* 20 (1993) 113–133.
[5] M.S.T. De Freitas, R.L. Viana, Multistability, basin boundary structure, and chaotic behavior in a suspension bridge model, *International Journal of Bifurcation and Chaos* 14 (2004) 927–950.
[6] S.H. Doole, S.J. Hogan, A piecewise linear suspension bridge model: nonlinear dynamics and orbit continuation, *Dynamics and Stability of Systems* 11 (1996) 19–47.
[7] A.V. Dyskin, E. Pasternak, E. Pelinovsky, Modelling resonances in topological interlocking structures, in: F. Albermani, B. Daniel, J. Griffiths, D. Hargreaves, P. Meehan, A. Tan, M. Veidt (Eds.), *ACAM2007*, *Proceedings of the 5th Australasian Congress on Applied Mechanics*, Vol. 2, Brisbane, Australia, 10–12 December 2007, pp. 408–413.
[8] V.A. Lazaryan, L.A. Manashkin, A.V. Ryzhov, Starting one-dimensional mechanical systems with pretensioned shock absorbers, *Prikladnaya Mechanica* 5 (1968) 64–70.
[9] A. Rivola, P.R. White, Bispectral analysis of the bilinear oscillator with application to the detection of fatigue cracks, *Journal of Sound and Vibration* 216 (1998) 889–910.
[10] L. Adler, Double elasticity in drill cores under flexure, *International Journal of Rock Mechanics and Mining Sciences & Geomechanics Abstracts* 7 (1970) 357–370.
[11] M.B. Prime, D.W. Shevitz, Linear and nonlinear methods for detecting cracks in beams, *Proceedings of the 14th International Modal Analysis Conference*, Dearborn, MI, 1996, pp. 1437–1443.

[12] V. Lyakhovsky, Y. Hamiel, P. Ampuero, Y. Ben-Zion, Nonlinear damage rheology and wave resonance in rocks, *International Journal of Geophysics* 178 (2009) 910–920.
[13] T.G. Chondros, A.D. Dimarogonas, J. Yao, Vibration of a beam with a breathing crack, *Journal of Sound and Vibration* 239 (2001) 57–67.
[14] J.A. Brandon, O.N.L. Abraham, Counter-intuitive quasi-periodic motion in the autonomous vibration of cracked Timoshenko beams, *Journal of Sound and Vibration* 185 (1995) 415–430.
[15] Z.K. Peng, Z.Q. Lang, F.L. Chu, Numerical analysis of cracked beams using nonlinear output frequency response functions, *Computers & Structures* 86 (2008) 1809–1818.
[16] M.C. Teich, S.E. Keilson, S.M. Hanna, Models of non-linear vibration. II. Oscillator with bilinear stiffness, *Acta Oto-Laryngologica (Stockh)* (Suppl. 467) (1989) 249–256.
[17] E. Detournay, Personal communication, 2009.
[18] A.V. Dyskin, E. Pasternak, E. Pelinovsky, Coupled bilinear oscillators, their resonances and controlling parameters, in: K. Teh, I. Davies, I. Howard (Eds.), *Proceedings of the 6th Australasian Congress on Applied Mechanics, ACAM 6*, 12–15 December 2010, Perth, Paper 1170, 9 pp.
[19] S.W. Shaw, P.J. Holmes, A periodically forced piecewise linear oscillator, *Journal of Sound and Vibration* 90 (1983) 129–155.
[20] G.S. Whiston, The vibro-impact response of a harmonically excited and preloaded one-dimensional linear oscillator, *Journal of Sound and Vibration* 115 (1987) 303–319.
[21] A.B. Nordmark, Non-periodic motion caused by grazing incidence in impact oscillators, *Journal of Sound and Vibration* 2 (1991) 279–297.
[22] M. Wiercigroch, Modelling of dynamical systems with motion dependent discontinuities, *Chaos Solitons and Fractals* 11 (2000) 2429–2442.
[23] I.Yu. Solodov, B.A. Korshak, Instability, chaos, and "memory" in acoustic-wave–crack interaction, *Physical Review Letters* 88 (2002) 041303.
[24] I.Yu. Solodov, N. Krohn, G. Busse, CAN: an example of nonclassical acoustic nonlinearity in solids, *Ultrasonics* 40 (2002) 621–625.
[25] I.Yu. Solodov, J. Wackerl, K. Pfleiderer, G. Busse, Nonlinear self-modulation and subharmonic acoustic spectroscopy for damage detection and location, *Applied Physics Letters* 84 (2004) 5386–5388.
[26] Y. Ohara, T. Mihara, R. Sasaki, T. Ogata, S. Yamamoto, Y. Kishimoto, K. Yamanaka, Imaging of closed cracks using nonlinear response of elastic waves at subharmonic frequency, *Applied Physics Letters* 90 (2007) 011902.
[27] M.V. Kurlenya, V.N. Oparin, V.I. Vostrikov, Pendulum-type waves. Part II: Experimental methods and main results of physical modelling, *Journal of Mining Science* 32 (1996) 245–273.
[28] Z.K. Peng, Z.Q. Lang, S.A. Billings, Y. Lu, Analysis of bilinear oscillators under harmonic loading using nonlinear output frequency response functions, *International Journal of Mechanical Sciences* 49 (2007) 1213–1225.
[29] R.N. Miles, Spectral response of a bilinear oscillator, *Journal of Sound and Vibration* 163 (1993) 319–326.
[30] J. Ing, E. Pavlovskaia, M. Wiercigroch, An experimental study into the bilinear oscillator close to grazing, *Journal of Physics: Conference Series* 96 (2008) 012119.
[31] M.V. Zakrzhevsky, D.V. Iourtchenko, Influence of random phase modulation on chaotic response of a bilinear driven oscillator, *Physics Conference 2005*, St. Petersburg, Russia, 2005, pp. 553–555.
[32] S.W. Shaw, R.H. Rand, The transition to chaos in a simple mechanical system, *International Journal of Non-Linear Mechanics* 24 (1989) 41–56.
[33] G.X. Li, R.H. Rand, F.C. Moon, Bifurcation and chaos in a forced zero-stiffness impact oscillator, *International Journal of Non-Linear Mechanics* 25 (1990) 417–432.
[34] M.T. Mata-Jiménez, B. Brogliato, Analysis of PD and non-linear control of mechanical systems with dynamic backlash, *Journal of Vibration and Control* 8 (2002) 1–37.
[35] S. Lenci, G. Rega, Regular non-linear dynamics and bifurcations of an impacting system under general periodic excitation, *Nonlinear Dynamics* 34 (2003) 249–268.